Department of Energy
Washington, DC 20585

QA: N/A
DOCKET NUMBER: 63-001

January 19, 2010

ATTN: Document Control Desk
John H. (Jack) Sulima, Project Manager
Project Management Branch B
Division of High-Level Waste Repository Safety
Office of Nuclear Material Safety and Safeguards
U.S. Nuclear Regulatory Commission
EBB-2B2
11545 Rockville Pike
Rockville, MD 20852-2738

YUCCA MOUNTAIN - REQUEST FOR ADDITIONAL INFORMATION - SAFETY EVALUATION REPORT, VOLUME 3 - POSTCLOSURE CHAPTER 2.2.1.3.2, MECHANICAL DISRUPTION OF ENGINEERED BARRIERS, 3RD SET - (DEPARTMENT OF ENERGY'S SAFETY ANALYSIS REPORT SECTION 2.3.4)

Reference: Ltr, Sulima to Williams, dtd 12/14/2009, "Yucca Mountain – Request for Additional Information – Safety Evaluation Report, Volume 3 – Postclosure Chapter 2.2.1.3.2, Mechanical Disruption of Engineered Barriers, 3rd Set – (Department of Energy's Safety Analysis Report Section 2.3.4)"

The purpose of this letter is to transmit the U.S. Department of Energy's (DOE) responses to three (3) of the nine (9) Requests for Additional Information (RAI) identified in the above-referenced letter. The responses to RAI Numbers 2, 3, and 4 are provided as enclosures to this letter. DOE submitted the responses to RAI Numbers 5, 6, 8, and 9 on January 7, 2010; the response to RAI Number 7 on January 12; and expects to submit the remaining RAI response on or before January 27, 2010.

The DOE references cited in the RAI responses have previously been provided with the License Application (LA), the LA update, or as part of previous RAI responses. The reference provided with a previous RAI response is identified within the enclosed response reference section.

There are no commitments in the enclosed RAI responses. If you have any questions regarding this letter, please contact me at (202) 586-9620, or by email to jeff.williams@rw.doe.gov.

Jeffrey R. Williams, Supervisor
Licensing Interactions Branch
Regulatory Affairs Division
Office of Technical Management

OTM:CJM-0237

Enclosures (3):

Responses to RAI Volume 3, Chapter 2.2.1.3.2, Set 3, Numbers 2 through 4

Printed with soy ink on recycled paper

cc w/encls:
J. C. Chen, NRC, Rockville, MD
J. R. Cuadrado, NRC, Rockville, MD
J. R. Davis, NRC, Rockville, MD
R. K. Johnson, NRC, Rockville, MD
A. S. Mohseni, NRC, Rockville, MD
N. K. Stablein, NRC, Rockville, MD
D. B. Spitzberg, NRC, Arlington, TX
J. D. Parrott, NRC, Las Vegas, NV
L. M. Willoughby, NRC, Las Vegas, NV
Jack Sulima, NRC, Rockville, MD
Christian Jacobs, NRC, Rockville, MD
Lola Gomez, NRC, Rockville, MD
W. C. Patrick, CNWRA, San Antonio, TX
Budhi Sagar, CNWRA, San Antonio, TX
Bob Brient, CNWRA, San Antonio, TX
Rod McCullum, NEI, Washington, DC
B. J. Garrick, NWTRB, Arlington, VA
Bruce Breslow, State of Nevada, Carson City, NV
Alan Kalt, Churchill County, Fallon, NV
Irene Navis, Clark County, Las Vegas, NV
Ed Mueller, Esmeralda County, Goldfield, NV
Ron Damele, Eureka County, Eureka, NV
Alisa Lembke, Inyo County, Independence, CA
Chuck Chapin, Lander County, Battle Mountain, NV
Connie Simkins, Lincoln County, Pioche, NV
Linda Mathias, Mineral County, Hawthorne, NV
Darrell Lacy, Nye County, Pahrump, NV
Jeff VanNeil, Nye County, Pahrump, NV
Joe Kennedy, Timbisha Shoshone Tribe, Death Valley, CA
Mike Simon, White Pine County, Ely, NV
K. W. Bell, California Energy Commission, Sacramento, CA
Barbara Byron, California Energy Commission, Sacramento, CA
Susan Durbin, California Attorney General's Office, Sacramento, CA
Charles Fitzpatrick, Egan, Fitzpatrick, Malsch, PLLC

EIE Document Components:

001_Trans_Ltr_3.2.2.1.3.2_Set_3_RAI_2_3_4.pdf
002_Encl_3.2.2.1.3.2_Set_3_RAI_2_3_4.pdf 14,632 KB

RAI Volume 3, Chapter 2.2.1.3.2, Third Set, Number 2:

Demonstrate that the drip shield quasi-static limit load analyses appropriately represent the potential effects on drip shield performance from horizontal accelerations during vibratory ground motion from seismic events.

Basis: To obtain an approximation of the peak ground acceleration that the drip shield can withstand, the applicant monotonically increased the initial static vertical load, while keeping constant the lateral rubble loading (SNL, 2007ap; Section 6.4.3.2.2.2). The approach appears to be inconsistent with the dynamic loading being represented in the quasi-static analysis, given that dynamic amplifications in the horizontal accelerations are expected to be similar to those in the vertical direction, according to applicant's results (BSC, 2004al; Appendix P).

1. RESPONSE

1.1 INTRODUCTION

The quasi-static limit load analyses were used to estimate the drip shield fragility during the vibratory ground motion from seismic events. Quasi-static analysis is a good approximation of the interaction between the drip shield and the rubble (resulting from seismic-induced drift degradation) and of the dynamic amplification of rockfall load during a seismic event, which is the main cause of increased stress and potential failure of the drip shield. The comparison of the results of the quasi-static analyses with the results of the dynamic simulations of interaction between the drip shield and rubble, which include vertical and horizontal accelerations during seismic ground motions, confirms that the quasi-static analyses adequately represent drip shield performance and that horizontal accelerations have a secondary effect. The response to RAI 3.2.2.1.3.2-3-007 provides additional information about the comparison of the dynamic and quasi-static analyses of drip shield load capacity under seismically accelerated rubble loads. Even though the quasi-static approach creates an approximate representation of lateral loading, the comparison of results from the quasi-static approach and the dynamic simulations demonstrates that the quasi-static approach provides an adequate representation of drip shield failure for the drip shield fragility curves in the seismic scenario class. In addition, it is not appropriate to use the transient dynamic loads in a quasi-static analysis, as explained next.

The transient dynamic loads on the drip shield have been analyzed for each of 30 segments along the drip shield profile as documented in *Drift Degradation Analysis* (BSC 2004, Appendix P). This analysis shows that the values of the horizontal loads on the drip shield legs are similar to those of the vertical loads on the drip shield crown (BSC 2004, Figures P-8 and P-10 versus Figure P-9). These transient dynamic loads, and particularly the horizontal transient dynamic loads, are not appropriate for use as loads in the quasi-static analysis for drip shield stability for a couple of reasons. First, the transient loads are a consequence of the dynamic impacts and local interaction between the deforming drip shield and the seismically induced rockfall. The resulting forces can sometimes be high but have a brief duration, on the order of milliseconds (BSC 2004, Figures P-8 to P-10). Using those forces in quasi-static analysis, as permanent loads, would significantly overestimate the load on the drip shield. Second, the drip shield is assumed to be

elastic but with overestimated stiffness in the analyses as documented in *Drift Degradation Analysis* (BSC 2004, Appendix P). An elastic response minimizes structural deformation and thereby maximizes rockfall loads in comparison to an elastic-plastic response, with its potential for larger structural deformation that reduces the rockfall loading. Stated differently, an elastic analysis minimizes the rockfall/structure interaction that is a key element of the dynamic loading on the drip shield. Given those limitations, the resulting loads (BSC 2004, Appendix P) have not been used for assessment of drip shield stability during seismic ground motion. Instead, a dynamic analysis of the interaction between the drip shield and rubble, which includes representation of the strength of the drip shield components and an approximation of their elastic-plastic response (SNL 2007, Section 6.4.4), has been used to validate the quasi-static analyses of drip shield fragility.

1.2 LATERAL LOADS FROM QUASI-STATIC ANALYSIS

The failure loads of the drip shield framework are determined based on quasi-static simulations of the three-dimensional representation of a one-fifth segment of the drip shield subject to rubble load (SNL 2007, Section 6.4.3.2). The analyses were carried out for three drip shield configurations and two initial rubble load distributions: the mean rockfall load from six realizations of rockfall from seismic events and load realization 3, which had the maximum rubble load on the crown of the drip shield and is characterized as the most severe of the six (SNL 2007, Section 6.4.3.2.2.2 and Table 6-136).

In the analysis of the drip shield fragility, the vertical load on the drip shield crown is gradually and proportionally increased (because the load is not uniform in the cross section perpendicular to the drip shield axis) until the strain at any point of the drip shield reaches the rupture strain. The horizontal loads on the sides (legs) of the drip shield were not increased proportionally to the increase in the vertical load because the dynamic amplification from vertical accelerations during a seismic event will not directly increase the lateral loads on the sidewalls of the drip shield. This approach, the basis of which is discussed in more detail in Section 1.3, does not mean that the lateral loads are constant, as explained next.

The lateral loads changed as a result of the interaction between the drip shield legs and surrounding rubble. The rubble–sidewall interaction is represented by elastic springs whose stiffness is equivalent to the stiffness of the rubble accumulated between the drip shield legs and the drift walls. Figure 1 shows the typical contours of the reaction forces due to interaction between the drip shield and rubble for the case of the initial drip shield configuration and the average initial rubble pressure distribution (SNL 2007, Table 6-136). The rubble reaction forces can only be compressive (otherwise a gap is created), acting to compress the drip shield legs. In this particular case, the lower portion of the drip shield legs are moving inward (thus, no reaction forces there), while the upper portion, at the shoulders and below, is moving outward, resulting in rubble backpressure. The contours are shown for the quasi-static state in which the vertical load is magnified by a factor of 13.2 and the average vertical pressure is then calculated as 13.2×127.86 kPa = 1,688 kPa. (The initial average vertical rubble pressure on the drip shield crown, before amplification, is 127.86 kPa (SNL 2007, Table 6-136)). The maximum lateral load for this state can be calculated based on Figure 1. The maximum horizontal force is 818 N.

Considering the approximate zone edge length of the numerical grid is 0.03 m, the maximum lateral pressure is approximately:

$$p_{\max} = \frac{818\,\mathrm{N}}{0.03^2\,\mathrm{m}^2} = 909\,\mathrm{kPa} \qquad \text{(Eq. 1)}$$

This value can be compared to the average initial pressure on the left and right sides of the drip shield, 41.99 and 61.87 kPa, respectively (SNL 2007, Table 6-136). Thus, the lateral rubble load changes substantially during quasi-static analysis of the drip shield, and is about (909 kPa/1,688 kPa) = 54% of the vertical load for this state. The difference between the vertical and lateral loads is that the vertical load is an active load due to dynamic amplification of the rubble weight, while the lateral rubble load, as indicated by the contours of reaction forces shown in Figure 1, is a passive load due to pressure of the rubble against the deforming drip shield (as explained in detail in SNL 2007, Section 6.4.3.2.2.3).

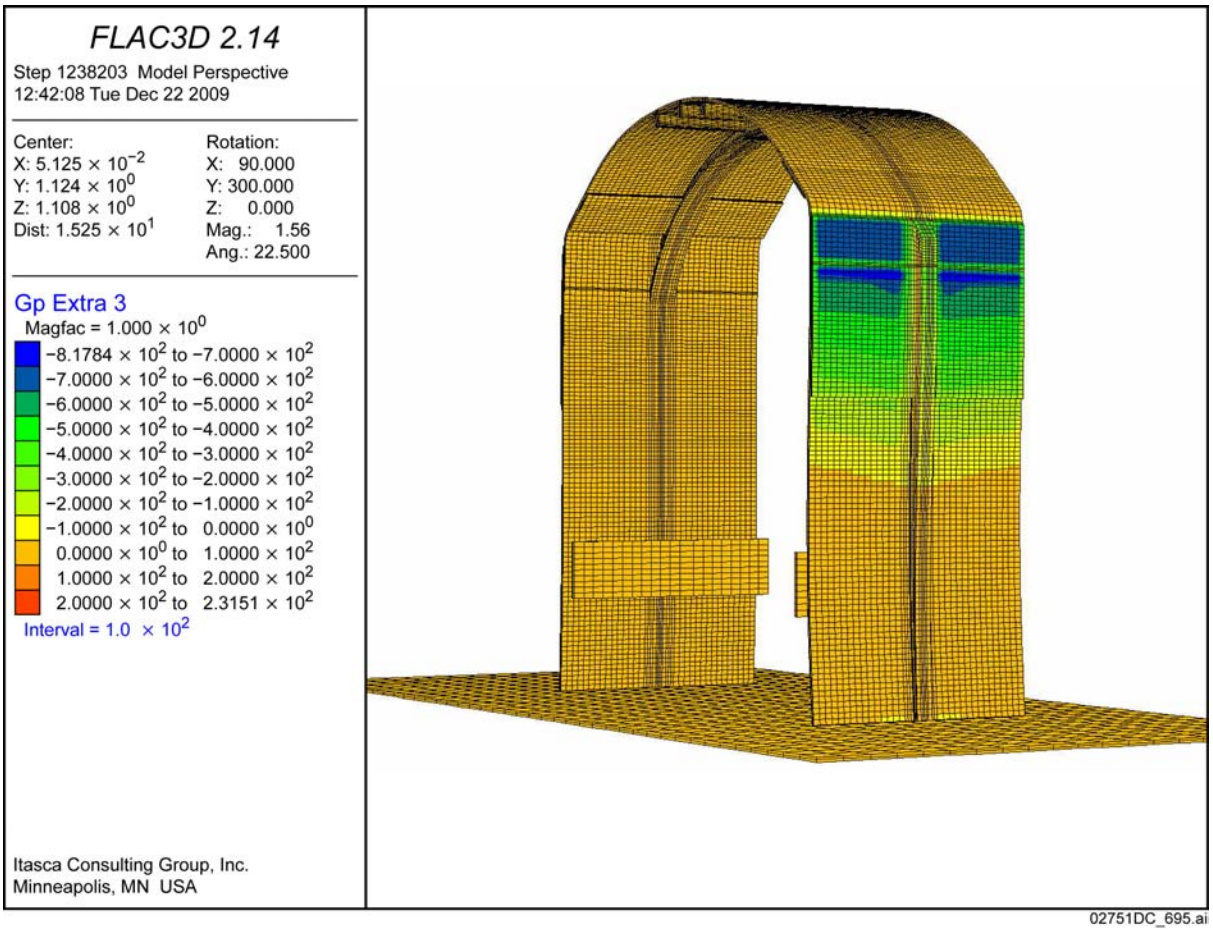

Figure 1. Contours of Reaction Forces (N) in a State during Quasi-Static Analysis for the Initial Thickness of the Drip Shield Components and Initial Average Rubble Load Distribution

1.3 QUASI-STATIC APPROXIMATION OF DYNAMIC RUBBLE LOADS

In the quasi-static analysis of the drip shield load-bearing capacity, the vertical loads were treated as active loads, while the lateral loads were treated as passive loads. Although the drift degradation involves some failure and unraveling of the drift walls, most of the caved rock accumulates above the drip shield (Figure 2). Thus, the predominant active rubble loading is the vertical loading on the drip shield crown. The active lateral load in the initial equilibrium state is a fraction of the vertical load. The large horizontal pressures in some of the rubble load realizations (SNL 2007, Table 6-136) are predominantly passive loads, the consequence of interaction between the drip shield structure and the surrounding rock. Any deformation and yielding of the drip shield, which is represented as elastic in the calculations of the rubble load (and, consequently, underestimates deformation of the drip shield and overestimates the lateral loads), will result in a decrease in the horizontal load. An elastic approximation does not allow yielding of the material. If stresses exceed the yield strength of the material, the elastic approximation will underestimate deformation. Typically, when the yield strength is exceeded, the deformation is governed by the tangent modulus, which is orders of magnitude smaller than the Young's modulus, which represents elastic deformation. The passive loads are functions of the stiffness of the materials in contact. An overestimate of the stiffness, or underestimate of deformation, will result in an overestimate of the passive loads.

Upward vertical acceleration will amplify the weight of the rock mass above the drip shield, and compress the drip shield against the relatively stiff invert. Although horizontal accelerations in the case of the seismic ground motions are approximately the same as the vertical accelerations, it is not expected that the horizontal acceleration will have any significant effect on the drip shield stability because, as shown in Figure 2, the mass of the failed rock mass accumulated along the drip shield legs is relatively small compared to the mass of the rock rubble above the drip shield.

Source: Created for illustrative purposes only.

Figure 2. Collapsed Emplacement Drift Internal Configuration

Another reason for the expected smaller effect of the horizontal acceleration compared to the vertical acceleration is the relatively stiff invert. The invert is relatively stiff in the vertical direction because it contains a small thickness of well graded and compacted crushed tuff in comparison to the rockfall surrounding the drip shield and because the crushed tuff is resting on top of intact rock. On the other hand, rubble conditions along the sides of the drip shield are assumed symmetrical. Because the drip shield is a free-standing structure, in the limiting case with no lateral constraints (i.e., no stable drift walls), the horizontal acceleration would cause similar lateral displacements of the drip shield and the rubble on both sides of the drip shield. The fluctuations of lateral forces on opposite sides of the drip shield will be approximately synchronous, resulting in no significant stresses in the drip shield. The drift wall on one side will provide some horizontal constraint, resulting in a displacement gradient in the horizontal direction and stress changes in the drip shield. However, because of the relatively compressible rubble along the drip shield sides versus the invert, those lateral forces will be smaller compared to the vertical forces on the crown of the drip shield that is supported by the relatively stiff invert.

To summarize, because the mass of rubble along the drip shield sides is relatively small and the drip shield is not pressed against a rigid lateral support (rather relatively loose rubble), the stresses induced by horizontal acceleration will be relatively small compared to the stresses

induced by vertical acceleration of the large rubble mass accumulated above the drip shield against the drip shield resting on the relatively stiff invert.

The quasi-static analysis therefore represents the main aspects of the drip shield–rubble interaction during seismic ground motions. The quasi-static analysis should underestimate the load-bearing capacity of the drip shield during strong seismic ground motion because the peak vertical ground acceleration occurs during a brief interval of time during a seismic ground motion while the quasi-static simulations assume the amplified vertical load is essentially constant. Also, the maximum vertical acceleration is used to assess rubble load amplification in the quasi-static analyses irrespective of its orientation, although only upward acceleration will cause an increase in the dynamic load. This reasoning suggests that the quasi-static analysis should overestimate the vertical loading on the drip shield and, therefore, underestimate the load-bearing capacity of the drip shield for a given peak vertical acceleration.

There is uncertainty in the quasi-static approximation because the interaction of the drip shield and surrounding rubble during seismic ground motions is a complex process, with the drip shield passing through a number of loading conditions and strain states. To confirm that the quasi-static analysis is adequate and generally underestimates the load-bearing capacity of the drip shield, its predictions are compared (SNL 2007, Section 6.4.4 and Table 6-146) with the results of 24 dynamic simulations for the 2.44 and 4.07 m/s peak ground velocity (PGV) levels and for three drip shield configurations (with 3 different levels of uniform corrosion). The four strongest ground motions from each PGV level (cases 4, 11, 13, and 17) were used in the dynamic analyses.

The dynamic simulations were carried out by applying the vertical component and the first horizontal component of each ground motion to a two-dimensional model. The seismic ground motions are defined by three time histories, two horizontal, H1 and H2, and one vertical. In the dynamic analyses, the H1 horizontal ground motion component is assumed to act perpendicular to the drift (drip shield) axis and is applied as a boundary condition to the model. The other horizontal component, H2, acts along the drift axis. It therefore has a second-order effect on drip shield–rubble interaction and, in any case, cannot be included in the two-dimensional representation for the dynamic analyses. The comparison with dynamic analyses (which includes horizontal acceleration) confirms that the quasi-static analysis and its approximation for the lateral loads (although it does not directly account for the effect of horizontal acceleration) provides a good approximation of the drip shield load-bearing capacity (SNL 2007, Section 6.4.4, Table 6-146). A more detailed discussion of quasi-static versus dynamic loading analyses is provided in the response to RAI 3.2.2.1.3.2-3-007.

1.4 DISCUSSION OF TRANSIENT RUBBLE PRESSURES

The transient rubble loads for 30 segments along the drip shield profile during seismic ground motions are calculated and reported in *Drift Degradation Analysis* (BSC 2004, Appendix P3). The calculations use ground-motion sets numbered 3, 7, 9, and 13 at the 2.44 and 5.35 m/s PGV levels, which correspond to the 10^{-6} and 10^{-7} annual exceedance probability on the unbounded seismic hazard (SNL 2007, Section C1). In those analyses, it is assumed that the drift is in the original configuration before it is subjected to strong seismic shaking. The effects of seismic

shaking on rubble pressures for 30 drip shield segments, in the case of an already collapsed drift, are reported in *Drift Degradation Analysis* (BSC 2004, Section P5). In this case, only one ground motion at 10^{-4}, 10^{-5}, and 10^{-6} annual exceedance probabilities (or, equivalently, the 0.4, 1.05, and 2.44 m/s PGV levels, respectively; SNL 2007, Section C1) was considered.

In all of the analyses reported in *Drift Degradation Analysis* (BSC 2004, Sections P3 and P5), the drip shield is assumed to be elastic and the stiffness of the legs was overestimated because thinning of the external support beams from the top (i.e., at the shoulder) to the bottom of the legs was ignored (i.e., the same support beam thickness was assumed over the entire height of the beam, from the top to the bottom of the drip shield sidewall). There are two consequences of these assumptions: (1) the analysis cannot be used for assessment of the potential for drip shield failure as a result of rupture of the drip shield components, and (2) the loads on the drip shield are overestimated (because stiffness and strength of the drip shield are overestimated).

The transient pressure histories show relatively large amplitudes (e.g., in excess of 35 MPa as shown in BSC 2004, Figure P-34, for ground-motion set 3 at 10^{-7} annual exceedance probability) of about the same value in the lateral and vertical directions (e.g., BSC 2004, Figures P-29 to P-31, for 10^{-6} ground motion). Those large pressure amplitudes are the result of local interactions during impact of the rock blocks into the drip shield. The predicted impact pressures are functions of the contact stiffness (between the blocks and the drip shield) used in the model. The calculations ignore the potential for complex, non-linear processes (i.e., the possible crushing of rock and yielding of titanium) to reduce the impact forces, resulting in a significant overestimate of the pressure amplitudes. The maximum impact energy of a single block during drift collapse in the lithophysal rock mass is 6.4 kJ/m (BSC 2004, Section P3) for 10^{-6} ground motion. (The results in BSC 2004, Appendix P, are for a two-dimensional model, which overestimates the impact energy because the out-of-plane dimension of blocks created by drift collapse in the lithophysal rock mass is a fraction of a meter.) The analysis for block impact in the nonlithophysal rock mass for greater block impact energies (SNL 2007, Section 6.4.7) has been carried out using a three-dimensional model and elasto-plastic constitutive relations for the rock block and drip shield components. These analyses indicate (SNL 2007, Tables 6-153, 6-155, and 6-156) that a 6.4-kJ block impact will not cause significant plastic strain or failure of the drip shield components.

The large pressure amplitudes are results of block impacts into the drip shield. The durations of pressure pulses caused by these impacts are typically on the order of one millisecond (BSC 2004, Section P3). Similar pressure amplitudes in the horizontal and vertical directions are consequences of similar horizontal and vertical accelerations and, consequently, impact velocities. However, the pressure amplitudes are not good indications of the dynamic strain and stress imposed on the structure as a whole or of the potential for failure of the drip shield during seismic events. The strain in the structure during the dynamic loading will also be a function of the duration of the loading and kinematic restraint in the direction of the loading (i.e., ability of the structure to resist the loading without the rigid body motion). Considering the relatively small mass and symmetrical conditions of rock rubble accumulated along the drip shield sides, the dynamically induced strain and stress in the drip shield by the horizontal acceleration will be smaller than those induced by the vertical acceleration.

The horizontal dynamic loads cannot be applied on the drip shield in the quasi-static analysis because the drip shield is a free-standing structure and its rigid body motion is not restrained in the horizontal direction. (The relatively rigid invert will restrain downward rigid-body motion of the drip shield.) Therefore, not only do horizontal dynamic loads have a less significant impact than do vertical loads, but horizontal dynamic loads are never in equilibrium (i.e., are not opposing and equal). Thus, a quasi-static analysis with horizontal dynamic loads is not realistic.

1.5 CONCLUSIONS

The main mechanism that can potentially cause failure of the drip shield during seismic ground motions is amplification of the rubble weight, predominantly accumulated above the drip shield, by vertical acceleration during a ground motion. The quasi-static limit load analysis adequately represents that mechanism. The quasi-static approach and assumptions used in that approach related to lateral loads are validated by comparison with the dynamic analyses of interaction between the drip shield and rubble, which include vertical and horizontal accelerations and the representation of strength and stress-strain response of the drip shield components.

2. COMMITMENTS TO NRC

None.

3. DESCRIPTION OF PROPOSED LA CHANGE

None.

4. REFERENCES

BSC (Bechtel SAIC Company) 2004. *Drift Degradation Analysis.* ANL-EBS-MD-000027 REV 03. Las Vegas, Nevada: Bechtel SAIC Company. ACC: DOC.20040915.0010; DOC.20050419.0001; DOC.20051130.0002; DOC.20060731.0005; LLR.20080311.0066.

SNL (Sandia National Laboratories) 2007. *Mechanical Assessment of Degraded Waste Packages and Drip Shields Subject to Vibratory Ground Motion.* MDL-WIS-AC-000001 REV 00. Las Vegas, Nevada: Sandia National Laboratories. ACC: DOC.20070917.0006; DOC.20080623.0002; DOC.20081021.0001.

RAI Volume 3, Chapter 2.2.1.3.2, Third Set, Number 3:

For the drip shield two-dimensional model subjected to acceleration time histories, demonstrate that a failure criterion based on the effective plastic strain at the end of the dynamic simulations is appropriate. In addition, demonstrate that the effective plastic strain from one event is considered in the analyses of subsequent events.

Basis: DOE uses the maximum effective plastic strains at the end of the time history analyses to evaluate the drip shield performance (SAR Section 2.3.4.5.3.3.3 and SAR Figure 2.3.4-85) but does not provide maximum effective strain-time and maximum effective plastic strain-time relationships.

DOE has not shown that the maximum effective plastic strains at the end of the simulation, as calculated in UDEC, appropriately represents the maximum effective plastic strains experienced by components subjected to cyclic loading, such that the tensile effective strain-failure criterion (SAR Section 2.3.4.5.1.2.2) is not underestimated.

1. RESPONSE

1.1 INTRODUCTION

The dynamic analysis of the drip shield surrounded by rubble (SNL 2007a, Section 6.4.4), investigated the potential for failure of the drip shield due to rupture or buckling of its Titanium Grades 7 and 29 components. Rupture potential at any location on the drip shield is assessed through the parameter of effective plastic strain, which accounts for the complete strain history during the seismic event.[1] The technical basis for using effective plastic strain to evaluate material failure for Alloy 22 is discussed in detail in the response to RAI 3.2.2.1.3.2-2-007. The same logic for Alloy 22 is also applicable to titanium, as explained in Section 1.2 of this response.

The potential to accumulate effective plastic strain from multiple seismic events has not been considered in the fragility curves for the drip shield sidewalls or for the drip shield plates. Conceptually, the cumulative effect of multiple seismic events, each producing a non-zero effective plastic strain less than the threshold for buckling or rupture, could drive a drip shield component to failure. However, the analysis presented in this response demonstrates: (1) the

[1] The term "seismic event" in this response generally refers to the ground motion caused by an earthquake. In the context of postclosure seismic consequence analyses, the ground motion is typically characterized by the peak velocity value of its first horizontal component, denoted as PGVH1. For a given value of PGVH1, the probabilistic seismic hazard analysis for Yucca Mountain, combined with ground motion conditioning and site-response modeling, gives a mean annual frequency with which the PGVH1 value is expected to be exceeded (the bounded hazard curve). Seismic event rates refer, therefore, to ground motion exceedance rates rather than earthquake occurrence rates.

amount of the effective plastic strain generated by lower-intensity seismic events is usually negligible compared to the failure strains associated with sidewall buckling or plate rupture, even when multiple events occur; and (2) less frequent, higher-intensity seismic events with the potential to cause significant levels of effective plastic strain have a very low probability of occurring multiple times during the period of interest. This response to multiple seismic events is consistent with a buckling process, wherein plastic strains remain very small until the load exceeds a limiting value that results in sudden failure with very large plastic strains.

1.2 EFFECTIVE PLASTIC STRAIN AS A METRIC TO ASSESS MATERIAL RUPTURE POTENTIAL

For ductile materials like titanium, ultimate tensile failure (rupture) was considered to occur when the effective strain (at any time during the dynamic simulation) exceeded a threshold value. (Note that Titanium Grade 24 was used in the calculations as a proxy for Titanium Grade 29, which is the design material for the drip shield framework (SNL 2007a, Section 4.1.5)). Because the drip shield plates were not explicitly included in the two-dimensional representation used for the dynamic analysis of the drip shield and because the rupture strain of Titanium Grade 24 is less than the rupture strain of Titanium Grade 7 (SNL 2007a, Tables 6-134, A-1, and A-2), only the rupture strain of Titanium Grade 24 was used in the analyses.

The effective strain is a scalar measure of strain related to the second invariant of deviatoric strain (SNL 2007a, Equation 6-6). The relationship for effective strain represents the general strain state (which is a tensor variable) as a scalar variable that is equal to the axial strain or elongation for uniaxial extension. An effective strain threshold when rupture occurs is defined based on elongation of Titanium 24. Because the large strains in the drip shield components are generally associated with bending of linear structural elements (such as the interior bulkheads and the large external support beams) that respond almost uniaxially, the rupture strain was not corrected by a triaxiality factor for a biaxial or triaxial stress state (as was done for Alloy 22 in SNL 2007a, Appendix A2).

In the dynamic analysis of a drip shield (SAR Section 2.3.4.5.3.3.3 and SNL 2007a, Section 6.4.4), the effective plastic strain, instead of the effective strain, was used in the assessment of the potential for rupture. Plastic strain is typically stored as a history variable during the analysis, and effective plastic strain is determined as the sum of effective plastic strain increments over time. The use of effective plastic strain in place of effective strain is justified because the difference between the two is insignificant for the case of monotonically increasing loading and conservative for cases with hysteretic response. However, because the effective plastic strain is used in place of effective strain, the rupture strain is reduced by the value of the elastic strain to ensure a conservative measure of rupture (SNL 2007a, Section 6.4.4.6). *Mechanical Assessment of Degraded Waste Packages and Drip Shields Subject to Vibratory Ground Motion* (SNL 2007a, Section A2, next-to-last paragraph) provides additional justification for use of the effective plastic strain instead of effective strain. Although the discussion relates to Alloy 22, the justification is applicable to Titanium Grade 29, which is the material specified in the license application design for the drip shield framework (SNL 2007a, Section 4.1.5).

In the response to RAI 3.2.2.1.3.2-2-007, the relationship between the effective strain and the effective plastic strain is explained in more detail. That response demonstrates that the effective plastic strain is a non-decreasing, non-negative variable, and its value at the end of simulation underestimates the maximum effective strain by the amount of the elastic strain in the case of monotonically increasing strain histories. The response also showed that the effective plastic strain typically overestimates the maximum effective strain (achieved at any time during the dynamic simulation) in the case of cyclic strain histories. The response to RAI 3.2.2.1.3.2-2-007 also provides an example from an actual simulation confirming that the effective plastic strain is always greater than the effective strain at any time during the simulation.

The structural analyses for drip shield response begin from an initial state with zero plastic strain. Because the initial plastic strain is zero, the individual calculations do not represent the response of a previously damaged drip shield during multiple seismic events.

1.3 BUCKLING PROCESS FOR THE DRIP SHIELD FRAMEWORK

The abstraction for the fragility of the drip shield sidewalls, as described in the second paragraph of SAR Section 2.3.4.5.3.4, is based on the ultimate plastic load capacity defined by the quasi-static three-dimensional finite-difference calculations described in SAR Section 2.3.4.5.3.3.2. The results from these quasi-static calculations are therefore an appropriate basis for describing the buckling process in this section and for determining the potential for effective plastic strain to accumulate from multiple seismic events in Sections 1.4 and 1.5.

Figure 1 illustrates the process of the buckling of the sidewalls for rubble load realization 3, based on the three-dimensional, quasi-static calculations. Load realization 3 was selected for the analysis because that realization results in the largest vertical load on the drip shield crown (SNL 2007a, Section 6.4.3.2.2.2 and Table 6-136). For a given thickness of the drip shield framework, effective plastic strain increases very slowly until a critical pressure is reached, at which point the sidewalls become unstable and the effective plastic strain increases abruptly by an order of magnitude or more. This abrupt strain increase is attributed to buckling. Note also that the effective plastic strain when the sidewall buckles is small relative to the ultimate tensile strain for Titanium Grade 24 (SNL 2007a, Table 6-134), which is shown as a solid black horizontal line near the top of Figure 1. (Titanium Grade 24 was used in the calculations as a proxy for Titanium Grade 29, which is the material for the drip shield framework in the current design (SNL 2007a, Section 4.1.5)).

The legend for Figure 1 presents the thickness reduction for the drip shield components. The thickness reductions of 0 mm (as-installed), 5 mm, and 10 mm represent the effect of general corrosion over long periods of time. These three states correspond to plate thicknesses of 15 mm (as-installed), 10 mm, and 5 mm, respectively. These thickness reductions therefore span a range of states, from the as-installed condition to a condition that is close to failure.

Table 1 presents the numerical data points that define each of the curves shown in Figure 1. Each curve includes a bend or “knee.” The “knee” represents the computational point with the greatest pressure before the sidewalls become unstable and the effective plastic strain increases

by approximately an order of magnitude (or more) for the next pressure increment in the quasi-static calculation. Inspection of Figure 1 confirms that the maximum effective plastic strain at the "knee" of each curve is quite small relative to 0.152, the ultimate plastic strain of Titanium Grade 24 (SNL 2007a Table 6-134). In other words, the effective plastic strain remains small until the pressure exceeds the critical pressure for buckling.

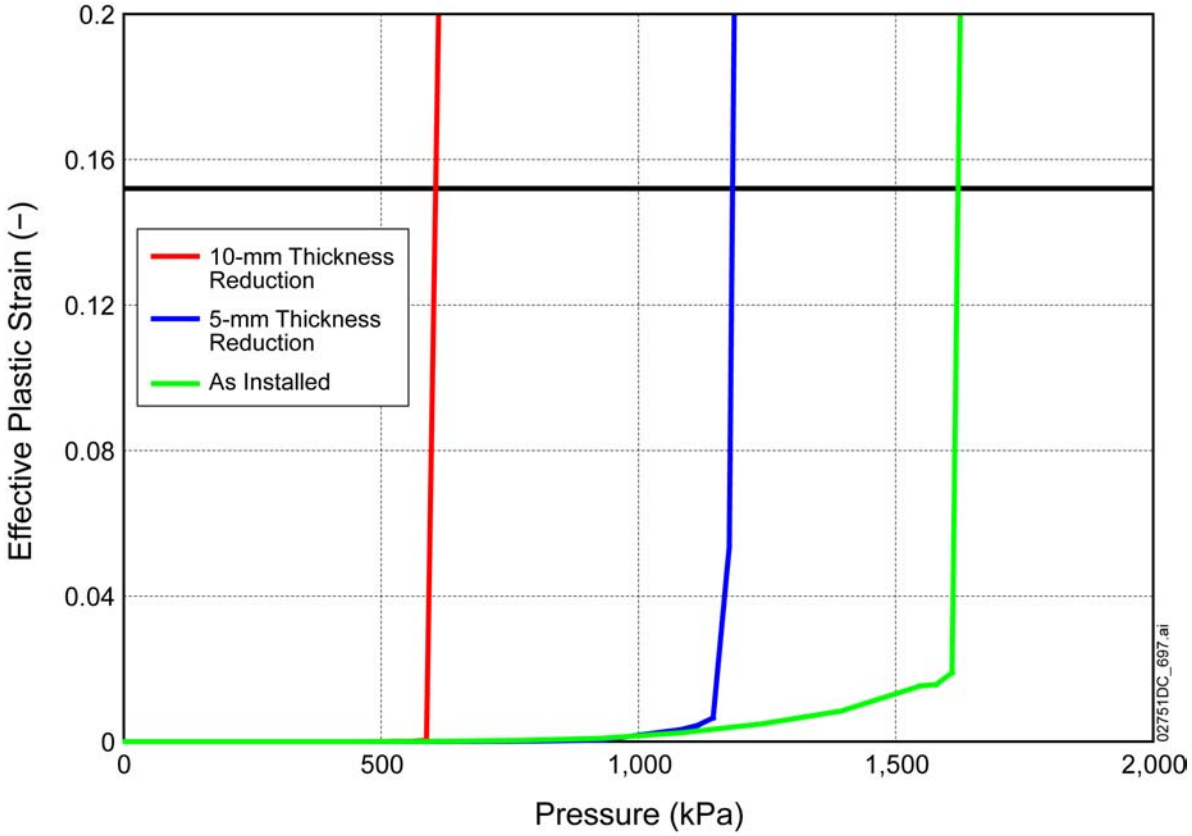

Source: SNL 2007a, Figure 6-53.

NOTE: The horizontal black line represents the ultimate plastic strain for Titanium Grade 24.

Figure 1. Maximum Effective Plastic Strain in the Drip Shield Framework as a Function of Load for Rubble Load Realization 3

Table 1. Maximum Effective Plastic Strain in the Drip Shield Framework for Rubble Load Realization 3

As-Installed		5-mm Thickness Reduction		10-mm Thickness Reduction	
Pressure (Pa)	Maximum Effective Plastic Strain (−)	Pressure (Pa)	Maximum Effective Plastic Strain (−)	Pressure (Pa)	Maximum Effective Plastic Strain (−)
0	0	0	0	0	0
1.55×10^5	0	1.55×10^5	0	1.55×10^5	0
3.10×10^5	0	3.10×10^5	0	3.10×10^5	0
4.64×10^5	0	4.64×10^5	0	4.64×10^5	0
6.19×10^5	8.40×10^{-5}	6.19×10^5	0	4.95×10^5	7.77×10^{-6}
7.74×10^5	3.62×10^{-4}	7.74×10^5	7.87×10^{-5}	5.26×10^5	4.63×10^{-5}
9.29×10^5	8.91×10^{-4}	9.29×10^5	3.71×10^{-4}	5.57×10^5	1.18×10^{-4}
1.08×10^6	2.41×10^{-3}	1.08×10^6	3.31×10^{-3}	5.88×10^5	3.17×10^{-4}
1.24×10^6	4.85×10^{-3}	1.11×10^6	4.42×10^{-3}	6.19×10^5	0.262
1.39×10^6	8.41×10^{-3}	1.15×10^6	6.49×10^{-3}		
1.55×10^6	0.0153	1.18×10^6	0.0535		
1.58×10^6	0.0157	1.21×10^6	0.5214		
1.61×10^6	0.0189				
1.64×10^6	0.3742				

Source: DTN: MO0701DRIPSHLD.000, *2_Drip_Shield_Framework_Fragility.zip*, *Summary.zip*, file: *summary load3.xls*, worksheet "DS frame."

1.4 CONTRIBUTION OF MULTIPLE SEISMIC EVENTS TO EFFECTIVE PLASTIC STRAIN FOR BUCKLING OF THE DRIP SHIELD FRAMEWORK

The data in Table 1 provide a basis for estimating the impact of multiple seismic events on the accumulation of effective plastic strain in the drip shield framework. This analysis has the following steps:

For a given quasi-static load curve in Figure 1, determine the equivalent values of the peak vertical ground acceleration (PGA_V). The values of PGA_V are then correlated with the horizontal component of peak ground velocity, PGV_{H1}. The correlation with PGV_{H1} is necessary because the bounded hazard curve defines the frequency of exceeding PGV_{H1} values, not PGA_V values.

Eliminate from the analysis values of PGV_{H1} that result in zero plastic strain or that result in buckling from a single earthquake. For values that result in zero plastic strain in a single earthquake, no accumulation of plastic strain occurs for multiple events. For values associated with buckling of the drip shield framework in a single event, accumulation of plastic strain from multiple events does not occur because the structure has already failed.

Divide the remaining range of values for PGV_{H1} into two parts: a range with higher exceedance frequencies (low-intensity events) and a range with lower exceedance frequencies (high-intensity events).

For each range, evaluate the maximum effective plastic strain from a seismic event and the frequency of occurrence of multiple seismic events.

Determine the amount of effective plastic strain that accumulates from multiple seismic events based on the maximum plastic strain and the expected frequency of such earthquakes occurring multiple times determined in step 4.

This approach assumes that the effective plastic strain from multiple seismic events is the sum of the effective plastic strain from the individual events. This is a conservative assumption because plastic deformation may not always occur at the same location on the drip shield and because any work hardening from a prior seismic event makes the material "tougher" during a subsequent event.

1.4.1 Equivalent Value of PGA_V and Correlated Value of PGV_{H1}

The quasi-static pressure on the drip shield, p_{qs}, can be interpreted as the sum of a static component due to the rockfall load and a dynamic component due to PGA_V:

$$p_{qs} = (1 + \frac{PGA_V}{g}) p_{static}, \qquad \text{(Eq. 1)}$$

where g is the acceleration of gravity and p_{static} is the static rockfall load on the crown of the drip shield. Because the bounded hazard curve is defined as a function of PGV_{H1}, rather than PGA_V, the PGA_V value is related to PGV_{H1} using a regression fit (SNL 2007b, Figure 6-64 and Equation 6.8-13):

$$\ln\left(\frac{PGA_V}{g}\right) = 1.1079 \ln(PGV_{H1}) + 0.3514, \qquad \text{(Eq. 2)}$$

which, for convenience, can be rewritten as:

$$\ln(PGV_{H1}) = \frac{\ln\left(\frac{PGA_V}{g}\right) - 0.3514}{1.1079}. \qquad \text{(Eq. 3)}$$

The regression fit for Equation 2 defines the mean value of $\ln(PGA_V)$ as a function of $\ln(PGV_{H1})$. In this situation, the full uncertainty in PGA_V is not represented (see SNL 2007b, Figure 6-64), but this is not a significant limitation on this analysis because the mean value is useful for estimating the expected number of seismic events that result in plastic strain.

For a value of PGA_V, a mean annual exceedance frequency is obtained using the bounded hazard curve (SNL 2007b, Table 6-3) and the corresponding PGV_{H1} value determined from the regression relation.

1.4.2 Analysis for the As-Installed Drip Shield

Table 2 presents the relevant calculations using the data in Table 1 for the as-installed drip shield (i.e., no thickness loss from general corrosion).

Table 2. Equivalent Values of PGA_V and PGV_{H1} for the As-Installed Drip Shield with Load Realization 3

Pressure (Pa)	Maximum Effective Plastic Strain (−)	PGA_V/g (−)	PGV_{H1} (m/s)	Annual Exceedance Frequency (λ, per year)
0	0	—	—	—
1.55×10^5	0	0.0	—	—
3.10×10^5	0	1.0	0.73	2.40×10^{-5}
4.64×10^5	0	2.0	1.36	4.22×10^{-6}
6.19×10^5	8.40×10^{-5}	3.0	1.96	9.38×10^{-7}
7.74×10^5	3.62×10^{-4}	4.0	2.54	3.82×10^{-7}
9.29×10^5	8.91×10^{-4}	5.0	3.11	1.36×10^{-7}
1.08×10^6	2.41×10^{-3}	6.0	3.67	3.59×10^{-8}
1.24×10^6	4.85×10^{-3}	7.0	4.22	5.58×10^{-9}

Source: File: MultiEvent Buckling Analysis for Drip Shield Framework – RAI 591.xls, worksheet "Frame – As Installed, Real 3."

The data in Table 2 demonstrate that seismic events with PGV_{H1} less than or equal to 1.36 m/s, do not cause plastic deformation of the drip shield. The data also demonstrate that seismic events with PGV_{H1} between 1.36 and 4.22 m/s cause a maximum effective plastic strain of 0.00485 per event. A PGV_{H1} value of 4.07 m/s has a mean annual exceedance frequency of 10^{-8} per year according to the bounded hazard curve (SNL 2007b, Section 6.4.3). Because the total system performance assessment, including the seismic scenario, is limited to consideration of features, events, and processes with a one or greater chance in 10,000 of occurring within 10,000 years, PGV_{H1} values greater than 4.07 m/s do not need to be considered.

The expected number of seismic events is calculated using the standard Poisson formulation for events that occur randomly in time (SNL 2007b, Section 6.7.1.7.1). For a PGV_{H1} range defined by PGV_{H1max} and PGV_{H1min}, with mean annual exceedance frequencies of λ_{max} and λ_{min}, respectively, the number of seismic events is given by $(\lambda_{max} - \lambda_{min})(\Delta T)$ for a Poisson process with events that occur randomly with a frequency $(\lambda_{max} - \lambda_{min})$ over ΔT years (SNL 2007b, Section 6.7.1.7.1). Values for λ_{max} and λ_{min} are obtained from Table 2. The duration, ΔT, is taken as 300,000 years because the probability of drip shield failure is effectively one after 300,000 years, based on the best estimate cumulative distribution function in SAR Figure 2.1-11(a).

The potential to accumulate plastic strain is estimated by splitting the PGV_{H1} range into two parts: from 1.36 to 3.11 m/s (low-intensity) and from 3.11 to 4.07 m/s (high-intensity):

- The expected number of events in the lower PGV_{H1} range is (4.22×10^{-6} per year – 1.36×10^{-7} per year)(300,000 years) = 1.23 events. The maximum increment of effective plastic strain within this range is 8.91×10^{-4} (Table 2), which is more than a factor of 20 less than the strain at the "knee" of the curve, 0.0189, and more than a factor of 170 less than the ultimate plastic strain of Titanium Grade 24, 0.152.

- The expected number of events in the upper range is (1.36×10^{-7} per year – 10^{-8} per year)(300,000 years) = 0.04 events. Even one such seismic event occurs very infrequently, so the accumulation of effective plastic strain from multiple events is negligible.

In summary, the low-intensity seismic events that could occur during the 300,000-year lifetime of the as-installed drip shield provide an insignificant contribution to total effective plastic strain relative to the strain level associated with buckling of the framework, and high-intensity seismic events occur infrequently enough that multiple events are unlikely.

1.4.3 Analysis for the Drip Shield with 5-mm Thickness Reduction

Table 3 provides the relevant calculations for the drip shield with a 5-mm thickness reduction for all components. The data in Table 3 demonstrate that seismic events with PGV_{H1} less than or equal to 1.96 m/s do not cause plastic deformation of the drip shield. The data also demonstrate that seismic events with PGV_{H1} between 1.96 and 3.89 m/s cause a maximum plastic strain of 0.00649 per event. Events with PGV_{H1} equal to or greater than 4.00 m/s are beyond the "knee" of the curve in Figure 1, and represent buckling of the drip shield sidewalls.

Table 3. Equivalent Values of PGA_V and PGV_{H1} for the Drip Shield with 5-mm Thickness Reduction of All Components and for Load Realization 3

Pressure (Pa)	Maximum Effective Plastic Strain (−)	PGA_V/g (−)	PGV_{H1} (m/s)	Annual Exceedance Frequency (λ, per year)
0	0			
1.55×10^5	0	0.0		
3.10×10^5	0	1.0	0.73	2.40×10^{-5}
4.64×10^5	0	2.0	1.36	4.22×10^{-6}
6.19×10^5	0	3.0	1.96	9.38×10^{-7}
7.74×10^5	7.87×10^{-5}	4.0	2.54	3.82×10^{-7}
9.29×10^5	3.71×10^{-4}	5.0	3.11	1.36×10^{-7}
1.08×10^6	3.31×10^{-3}	6.0	3.67	3.59×10^{-8}
1.11×10^6	4.42×10^{-3}	6.2	3.78	2.65×10^{-8}

Table 3. Equivalent Values of PGA_V and PGV_{H1} for the Drip Shield with 5-mm Thickness Reduction of All Components and for Load Realization 3 (continued)

Pressure (Pa)	Maximum Effective Plastic Strain (−)	PGA_V/g (−)	PGV_{H1} (m/s)	Annual Exceedance Frequency (λ, per year)
1.15×10^6	6.49×10^{-3}	6.4	3.89	1.87×10^{-8}
1.18×10^6	5.35×10^{-2}	6.6	4.00	1.32×10^{-8}
1.21×10^6	5.21×10^{-1}	6.8	4.11	8.54×10^{-9}

The expected number of seismic events that can cause plastic strain to accumulate in the drip shield but not buckle the sidewalls is given by $(\lambda_{max} - \lambda_{min})(\Delta T)$ for a Poisson process. Values for λ_{max} and λ_{min} are obtained from Table 3. The duration, ΔT, is taken as 200,000 years. While the drip shields generally fail by 300,000 years after closure, the state with 5-mm thickness reduction represents an intermediate state, after the thickness of the plates have been reduced by one-third of their initial thickness, so the duration is also reduced by one-third.

The potential to accumulate plastic strain is estimated by splitting the PGV_{H1} range into two parts: from 1.96 to 3.11 m/s (low-intensity), and from 3.11 to 4.00 m/s (high-intensity), and by comparing the incremental plastic strains with the ultimate plastic strain of Titanium Grade 24, 0.152, or with the effective plastic strain at the "knee" in Figure 1 for the drip shield with a 5-mm thickness reduction, 6.49×10^{-3}:

- The expected number of events in the lower PGV_{H1} range is (9.38×10^{-7} per year – 1.36×10^{-7} per year)(200,000 years) = 0.16 events. The maximum increment of effective plastic strain within this range is 3.71×10^{-4} (Table 3), which is more than a factor of 17 less than the strain at the "knee" of the curve, 6.49×10^{-3}, and more than a factor of 400 less than the ultimate plastic strain of Titanium Grade 24, 0.152.

- The expected number of events in the upper range is (1.36×10^{-7} per year – 1.32×10^{-8} per year) (200,000 years) = 0.02 events. Even one such seismic event occurs very infrequently in the upper PGV_{H1} range, so the accumulation of effective plastic strain from multiple events is negligible.

In summary, the low-intensity seismic events that could occur relatively frequently during the 200,000-year period provide a negligible contribution to total effective plastic strain relative to the strain associated with buckling of the framework, and high-intensity seismic events occur infrequently enough that multiple events are unlikely.

1.4.4 Analysis for the Drip Shield with 10-mm Thickness Reduction

Table 4 provides the relevant calculations for the drip shield with a 10-mm thickness reduction for all components. The data in Table 4 demonstrate that seismic events with PGV_{H1} less than or equal to 1.36 m/s, do not cause plastic deformation of the drip shield. The data also demonstrate that seismic events with PGV_{H1} between 1.36 and 1.84 m/s cause a maximum plastic strain of

0.000317 per event. Events with PGV_{H1} equal to or greater than 1.96 m/s are beyond the "knee" of the curve in Figure 1, and represent buckling of the drip shield sidewalls.

Table 4. Equivalent Values of PGA_V and PGV_{H1} for the Drip Shield with 10-mm Thickness Reduction of All Components and for Load Realization 3

Pressure (Pa)	Maximum Effective Plastic Strain (–)	PGA_V/g (–)	PGV_{H1} (m/s)	Annual Exceedance Frequency (λ, per year)
0	0			
1.55×10^5	0	0.0		
3.10×10^5	0	1.0	0.73	2.40×10^{-5}
4.64×10^5	0	2.0	1.36	4.22×10^{-6}
4.95×10^5	7.77×10^{-6}	2.2	1.48	2.96×10^{-6}
5.26×10^5	4.63×10^{-5}	2.4	1.60	2.11×10^{-6}
5.57×10^5	1.18×10^{-4}	2.6	1.73	1.55×10^{-6}
5.88×10^5	3.17×10^{-4}	2.8	1.84	1.18×10^{-6}
6.19×10^5	2.62×10^{-1}	3.0	1.96	9.38×10^{-7}

The expected number of seismic events that can cause plastic strain to accumulate in the drip shield but not fail the drip shield is given by $(\lambda_{max} - \lambda_{min})(\Delta T)$ for a Poisson process. Values for λ_{max} and λ_{min} are obtained from Table 4. The duration, ΔT, is taken as 100,000 years because the drip shield plates have corroded to two-thirds of their original thickness, so the duration is also reduced to two thirds of the original value of 300,000 years.

The potential to accumulate plastic strain is estimated by splitting the PGV_{H1} range into two parts: from 1.36 to 1.60 m/s (low-intensity), and from 1.60 to 1.96 m/s (high-intensity), and by comparing the incremental plastic strains with the ultimate plastic strain of Titanium Grade 24, 0.152, or with the effective plastic strain at the "knee" in Figure 1 for the drip shield with a 10-mm thickness reduction, 3.17×10^{-4} (see Table 4):

- The expected number of events in the lower PGV_{H1} range is (4.22×10^{-6} per year – 2.11×10^{-6} per year)(100,000 years) = 0.21 events. The maximum increment of effective plastic strain within this range is 4.63×10^{-5} (see Table 4), which is about a factor of 7 less than the strain at the "knee" of the curve, 3.17×10^{-4}, and more than a factor of 3,000 less than the ultimate plastic strain of Titanium Grade 24, 0.152.

- The expected number of events in the upper range is (2.11×10^{-6} per year – 9.38×10^{-7} per year)(100,000 years) = 0.12 events. Two or more such seismic events occur very infrequently and therefore make negligible contributions to the accumulation of effective plastic strain from multiple events.

1.5 CONTRIBUTION OF MULTIPLE SEISMIC EVENTS TO EFFECTIVE PLASTIC STRAIN FOR BUCKLING WITH THE MEAN ROCKFALL LOAD AND FOR RUPTURE OF THE DRIP SHIELD PLATES

An analysis similar to that presented in Section 1.4 has been performed for the buckling of the drip shield framework for the mean load from six rockfall realizations and for the rupture of the drip shield plates with two boundary conditions (fixed and laterally free). Tables A-1 and A-2 summarize the key numerical results of the analysis for the buckling of the framework and rupture of the drip shield plates, respectively. The analysis generally concludes that the accumulation of plastic strain from multiple seismic events is negligible and does not result in an increase in failure from multiple events compared to single events. The basis for this result is similar to the conclusions in Sections 1.4.2 to 1.4.4: the low-intensity seismic events that could occur relatively frequently provide an insignificant contribution to total effective plastic strain relative to the strain associated with rupture of the plates, and the higher-intensity seismic events occur infrequently enough that multiple events are unlikely.

The single exception to this conclusion occurs for buckling of the framework with a 10-mm thickness reduction in all components and the mean rockfall load (see the last entry in Table A-1). In this case, positive plastic strain occurs for small pressure loads and could accumulate to a level that causes buckling from multiple seismic events. In this situation, the drip shield sidewalls would buckle sooner than predicted by the fragility curves for the drip shield framework. However, this change is not significant for overall system performance because:

- Significant levels of plastic strain do not accumulate for the as-installed drip shield and for the drip shield whose component thicknesses have been reduced by 5 mm. It follows that significant levels of plastic strain can only accumulate during the last one-third of the drip shield's lifetime, or from approximately 200,000 to 300,000 years after repository closure (see SAR Figure 2.1-11(a) for the lifetime of the drip shield).

- A sensitivity analysis has demonstrated that the timing of drip shield failure from wider uncertainty in titanium corrosion rates has a negligible effect on the mean annual dose (response to RAI 3.2.2.1.3.1-005). Changes in the general corrosion rate of titanium that alter the timing of drip shield failure may result in complex changes to the results of performance assessment, depending on the sequence of waste package failure times and drip shield failure times. The sensitivity study therefore considered both slower and faster general corrosion rates for titanium through the use of an uncertainty factor between 0.5 and 4. The resulting drip shield failure times varied between about 80,000 and 500,000 years (response to RAI 3.2.2.1.3.1-005, Figure 1), although the resulting mean annual dose varied by less than 1% from the mean annual dose without the uncertainty factor. If significant levels of plastic strain accumulate during the last one-third of a drip shield's lifetime, from 200,000 years to 300,000 years, the resulting changes in mean annual dose are expected to be on the order of 1% or less, and therefore negligible. Further details on the sensitivity analysis are documented in the response to RAI 3.2.2.1.3.1-005.

1.6 CONCLUSION

The maximum effective plastic strain at the end of a simulation is a good representation of, or overestimates, the maximum effective strain throughout the cyclic loading history. In the case of a monotonically increasing strain history, the effective plastic strain underestimates the effective strain by the value of the elastic strain, which is a relatively small fraction of the rupture strain. In the case of cyclic loading history, the value of the effective plastic strain at the end of simulation overestimates the effective strain at any time during the simulation. A failure criterion based on the effective plastic strain at the end of dynamic simulations is appropriate and typically would be expected to overestimate the failure potential for the drip shield.

A detailed analysis of the potential impact of multiple seismic events on the cumulative effective plastic strain demonstrates that the impact is generally not significant because the more frequent low-intensity seismic events have a negligible contribution to the total effective plastic strain, even with multiple seismic events, and because the infrequent, higher-intensity seismic events have a low probability of multiple events during the time period of interest. This statement is true for a buckling process because the effective plastic strain remains extremely small until a critical pressure is reached, as illustrated in Figure 1. For the one case where plastic strain can accumulate from multiple events, a negligible effect is expected on the mean annual dose from the total system performance assessment.

2. COMMITMENTS TO NRC

None.

3. DESCRIPTION OF PROPOSED LA CHANGE

None.

4. REFERENCES

Hahn, G.J. and Shapiro, S.S. 1967. *Statistical Models in Engineering.* New York, New York: John Wiley & Sons.

SNL (Sandia National Laboratories) 2007a. *Mechanical Assessment of Degraded Waste Packages and Drip Shields Subject to Vibratory Ground Motion.* MDL-WIS-AC-000001 REV 00. Las Vegas, Nevada: Sandia National Laboratories. ACC: DOC.20070917.0006; DOC.20080623.0002; DOC.20081021.0001; DOC.20090917.0002[a].

SNL 2007b. *Seismic Consequence Abstraction.* MDL-WIS-PA-000003 REV 03 Las Vegas, Nevada: Sandia National Laboratories. ACC: DOC.20070928.0011.

NOTE: [a]Provided as an enclosure to letter from Williams to Sulima dtd 01/07/2010. "Yucca Mountain – Request for Additional Information – Safety Evaluation Report, Volume 3 – Postclosure Chapter 2.2.1.3.2, Mechanical Disruption of Engineered Barriers, 3rd Set – (Department of Energy's Safety Analysis Report Section 2.3.4)."

APPENDIX A – SUMMARY TABLES

Table A-1. Summary of Multi-Event Analysis for Accumulation of Plastic Strain in the Drip Shield Framework

	Range of PGV-H1 (m/s)	Maximum Plastic Strain per Event (−)	$\Delta\lambda$ for This PGV-H1 Interval (per year)	Expected Number of Events (−)	Conclusion
Load Realization 3					
As-Installed	1.36 to 3.11	8.91×10^{-4}	4.09×10^{-6}	1.23	Multiple seismic events have no impact on buckling because the maximum increment in effective plastic strain per event, 8.91×10^{-4}, is much less than the ultimate tensile strain, 0.152, and much less than the strain at the "knee" just before buckling, 0.0189.
	3.11 to 4.07	4.85×10^{-3}	1.26×10^{-7}	0.04	Multiple seismic events have no impact on buckling because even one seismic event occurs very infrequently in this PGV range. A single, intense seismic event may rupture the plates, but no plastic strain accumulates from multiple events.
5-mm Thickness Reduction	1.96 to 3.11	3.71×10^{-4}	8.01×10^{-7}	0.16	Multiple seismic events have no impact on buckling because one or more seismic events occur very infrequently in this PGV range, because the maximum increment in effective plastic strain per event, 3.71×10^{-4}, is much less than the ultimate tensile strain, 0.152, and much less than the strain at the "knee" just before buckling, 6.49×10^{-3}.
	3.11 to 4.00	5.35×10^{-2}	1.23×10^{-7}	0.02	Multiple seismic events have no impact on buckling because even one seismic event occurs very infrequently in this PGV range. A single, intense seismic event may rupture the plates, but no plastic strain accumulates from multiple events.
10-mm Thickness Reduction	1.36 to 1.60	4.63×10^{-5}	2.11×10^{-6}	0.21	Multiple seismic events have no impact on buckling because the maximum increment in effective plastic strain per event, 4.63×10^{-5}, is much less than the ultimate tensile strain, 0.152, and much less than the strain at the "knee" just before buckling, 3.17×10^{-4}.
	1.60 to 1.96	2.62×10^{-1}	1.17×10^{-6}	0.12	Multiple seismic events have no impact on buckling because two or more intense seismic events occur very infrequently in this PGV range. A single, intense seismic event may rupture the plates, but no plastic strain accumulates from multiple events.
Mean Load from Six Rockfall Realizations					
As-Installed	1.96 to 4.07	7.21×10^{-4}	9.28×10^{-7}	0.28	Multiple seismic events have no impact on buckling because there are few multiple events, and because the max increment in effective plastic strain per event, 7.21×10^{-4}, is much less than the ultimate tensile strain, 0.152, and much less than the strain at the "knee" just before buckling, 0.0184.

Table A-1. Summary of Multi-Event Analysis for Accumulation of Plastic Strain in the Drip Shield Framework (continued)

	Range of PGV-H1 (m/s)	Maximum Plastic Strain per Event (−)	$\Delta\lambda$ for This PGV-H1 Interval (per year)	Expected Number of Events (−)	Conclusion
Mean Load from Six Rockfall Realizations					
5-mm Thickness Reduction	3.11 to 4.07	9.81×10^{-4}	1.26×10^{-7}	0.03	Multiple seismic events have no impact on buckling because one or more intense seismic events occur very infrequently in this PGV range. A single, intense seismic event may rupture the plates, but no plastic strain accumulates from multiple events.
10-mm Thickness Reduction	0.219 to 0.73	9.89×10^{-3}	4.05×10^{-4}	40.47	The maximum increment in effective plastic strain per event, 9.89×10^{-3}, is a factor of five less than the strain at the "knee" just before buckling, 4.77×10^{-2}. However, with 40 expected events, plastic strain could accumulate from multiple events.
	0.73 to 1.96	4.77×10^{-2}	2.31×10^{-5}	2.31	With two expected events, a significant amount of plastic strain can accumulate from multiple events.

Source: *MultiEvent Buckling Analysis for Drip Shield Framework.xls*, worksheet "Summary Table."

Table A-2. Summary of Multi-Event Analysis for Accumulation of Plastic Strain in the Drip Shield Plates

	Range of PGV-H1 (m/s)	Maximum Plastic Strain Per Event (−)	$\Delta\lambda$ for This PGV-H1 Interval (per year)	Expected Number of Events (−)	Conclusion
Case 1 (Fixed Boundary Conditions on Plate)					
As-Installed (15-mm-thick plate)	1.10 to 4.07	1.43×10^{-3}	8.59×10^{-6}	2.58	Multiple seismic events have no impact on plate rupture because the maximum increment in effective plastic strain per event, 1.43×10^{-3}, is much less than the ultimate tensile strain, 0.217.
10-mm-thick Plate	1.10 to 4.07	4.19×10^{-3}	8.59×10^{-6}	1.72	Multiple seismic events have no impact on plate rupture because the maximum increment in effective plastic strain per event, 4.19×10^{-3}, is much less than the ultimate tensile strain, 0.217.
5-mm-thick Plate	0.69 to 2.27	4.96×10^{-3}	2.71×10^{-5}	2.71	Multiple seismic events have no impact on plate rupture because the maximum increment in effective plastic strain per event, 4.96×10^{-3}, is much less than the ultimate tensile strain, 0.217.
	2.27 to 3.66	2.02×10^{-1}	5.40×10^{-7}	0.05	Multiple seismic events have no impact on buckling because one or more intense seismic events occur very infrequently in this PGV range. A single, intense seismic event may rupture the plates, but little plastic strain accumulates from multiple events.
Case 2 (Laterally Free Boundary Conditions on Plate)					
As-Installed (15-mm-thick plate)	2.64 to 4.07	2.71×10^{-5}	3.16×10^{-7}	0.09	Multiple seismic events have no impact on plate rupture because there are very few multiple events and because the maximum increment in effective plastic strain per event, 2.71×10^{-5}, is much less than the ultimate tensile strain, 0.217.
10-mm-thick Plate	1.89 to 4.07	2.58×10^{-3}	1.07×10^{-6}	0.21	Multiple seismic events have no impact on plate rupture because there are very few multiple events and because the maximum increment in effective plastic strain per event, 2.58×10^{-3}, is much less than the ultimate tensile strain, 0.217
5-mm-thick Plate	0.24 to 1.50	1.02×10^{-3}	3.43×10^{-4}	34.26	Multiple seismic events have no impact on plate rupture because the maximum increment in effective plastic strain per event, 1.02×10^{-3}, is much less than the ultimate tensile strain, 0.217.
	1.50 to 2.64	9.79×10^{-3}	2.49×10^{-6}	0.25	Multiple seismic events have no impact on buckling because one or more intense seismic events occur very infrequently in this PGV range. A single, intense seismic event may rupture the plates, but little plastic strain accumulates from multiple events.

Source: *MultiEvent Failure Analysis for Drip Shield Plates – RAI 591.xls*, worksheet "Summary Table."

RAI Volume 3, Chapter 2.2.1.3.2, Third Set, Number 4:

Demonstrate that including the base of the emplacement pallet in the dynamic analyses of drip shield mechanical performance does not overestimate drip shield capacity during vibratory ground motions.

Basis: DOE dynamic analyses in SAR section 2.3.4.5.3.3.3 include the waste package base pallet in the two dimensional model (e.g., SAR Figure 2.3.4-84). Some of the results of these analyses show that deformation of the drip shield sidewall may be influenced by the presence of the base pallet (e.g., SAR Figure 2.3.4-85). However, the base pallet only extends across approximately one fifth of the drip shield length. DOE analyses have not discussed the potential effects of drip shield-base pallet interactions during dynamic analyses, and have not included analyses in which the drip shield framework performance is not be influenced by the base pallet.

1. RESPONSE

1.1 INTRODUCTION

As illustrated in Figure 1, the emplacement pallet is included in the dynamic analysis of drip shield mechanical performance (SNL 2007a, Section 6.4.4). In this two-dimensional representation, the emplacement pallet extends along the entire length of the drip shield. Figure 2 illustrates the actual, three-dimensional geometry of the standard emplacement pallet, the drip shield, and the waste package. The standard emplacement pallet, which accounts for approximately 90% of the pallets in the repository, consists of two waste package supports (sometimes called cradles or pallet bases) connected by four stainless steel tubes (two on each side of the pallet) as shown in Figure 3. Although the two waste package supports included in one pallet extend along approximately 20% of the shield length (i.e., length of one waste package support is 0.5429 m compared to 5.805 m drip shield length), the entire standard emplacement pallet (4.148 m long) extends along 71% of the total drip shield length.

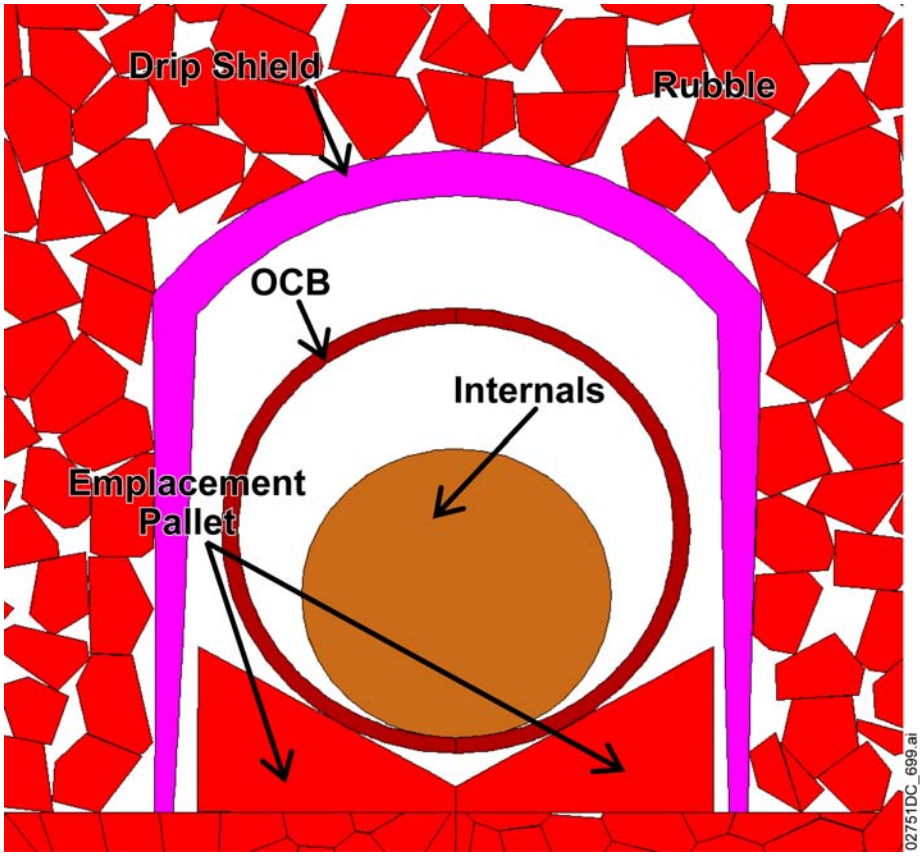

Source: Created for illustrative purposes only.

Figure 1. Geometrical Representation Used in the Analysis of the Mechanical Interaction between the Drip Shield and the Rubble during Seismic Ground Motions Shown on the Drip Shield Scale

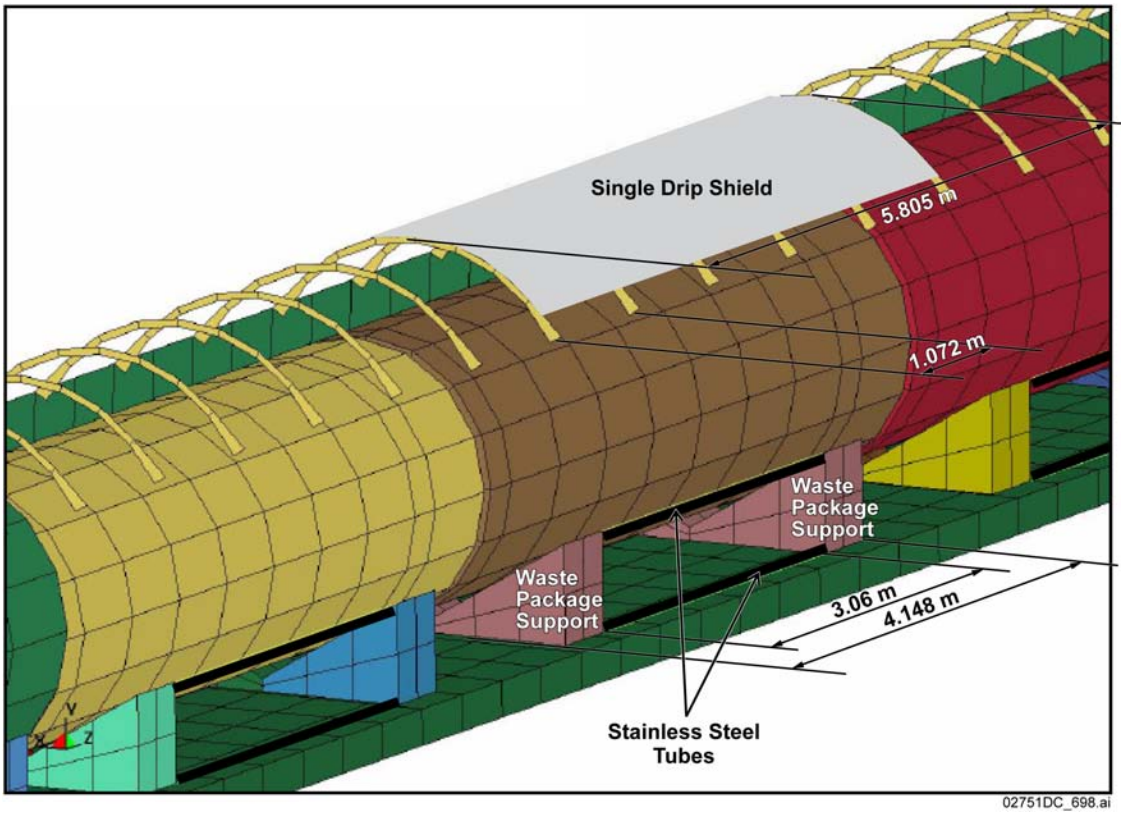

Source: Created for illustrative purposes only.

Figure 2. Illustration of the Drip Shield and the Standard Emplacement Pallet with Relevant Dimensions

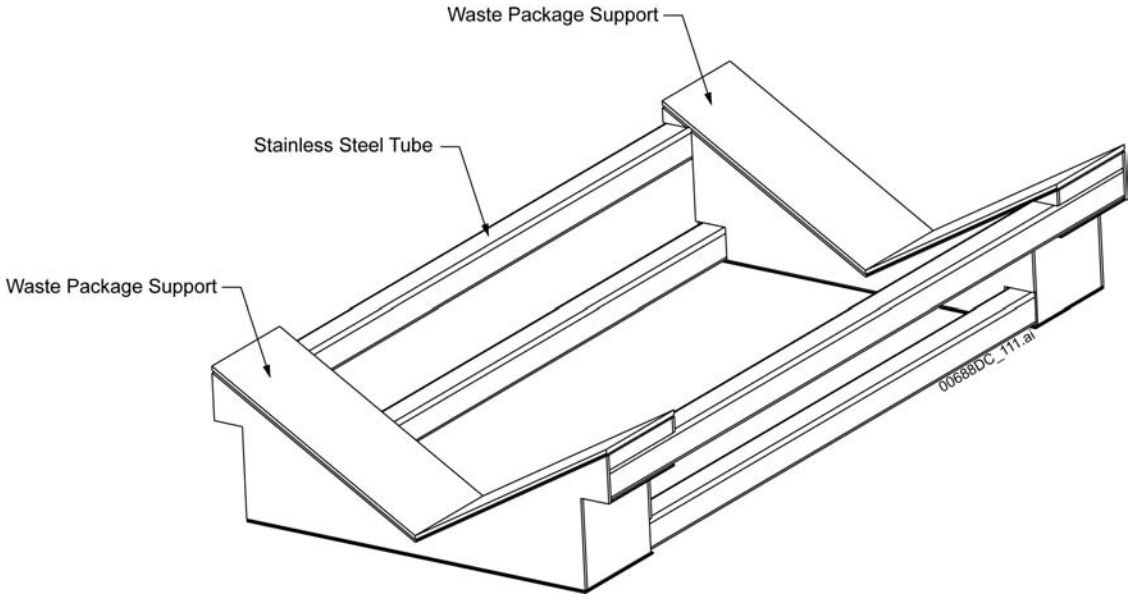

Source: Created for illustrative purposes only.

Figure 3. Illustration of the Standard Emplacement Pallet

One of the main objectives of the two-dimensional dynamic simulations of the interaction between the drip shield and the rubble (SNL 2007a, Section 6.4.4) was to demonstrate that the three-dimensional quasi-static fragility calculations adequately represent the drip shield load bearing capacity during vibratory ground motions. The results of the demonstration are summarized in Table 1 (reproduced from SAR Table 2.3.4-42), where the responses of the drip shield to dynamic seismic shaking and the quasi-static load are compared.

Table 1. Comparison of the Drip Shield Stability Assessment Based on Two-Dimensional Dynamic and Three-Dimensional Quasi-Static Analyses

				Initial Configuration (15-mm plate thickness)		5-mm-Thinned Configuration (10-mm plate thickness)		10-mm-Thinned Configuration (5-mm plate thickness)	
Case	PGV Level (m/s)	Vertical PGA (g)	Ultimate Load p_{ul} (kPa)	Fragility Analysis[a]	Dynamic Analysis	Fragility Analysis[b]	Dynamic Analysis	Fragility Analysis[c]	Dynamic Analysis
4	2.44	6.53	963	Stable	Stable	Stable	Stable	Fails	Stable
11	2.44	7.81	1,126	Stable	Stable	Fails	Stable	Fails	Fails
13	2.44	3.14	529	Stable	Stable	Stable	Stable	Fails	Stable
17	2.44	12.87	1,773	Fails	Stable	Fails	Stable	Fails	Stable
4	4.07	13.31	1,830	Fails	Stable	Fails	Stable	Fails	Fails
11	4.07	15.93	2,165	Fails	Fails	Fails	Fails	Fails	Fails
13	4.07	6.41	947	Stable	Fails	Stable	Fails	Fails	Fails
17	4.07	26.26	3,485	Fails	Fails	Fails	Stable	Fails	Fails

Source: SAR Table 2.3.4-42 and SNL 2007a, Table 6-146.

[a] Load Limit = 1,698 kPa.
[b] Load Limit = 1,094 kPa.
[c] Load Limit = 501 kPa.

NOTE: PGA = peak ground acceleration; PGV = peak ground velocity. The table entries under Dynamic Analysis columns with “Fails” were not evaluated further in this RAI response.

The two-dimensional modeled configuration for the drip shield and pallet contained geometrical simplifications of the system, some that tended to overestimate, and some that underestimated, the structural robustness of the system in the dynamic analyses. As noted in the RAI question, the inclusion of the pallet as a restraint to lateral and inward movement of drip shield legs can lead to an overestimate. But as noted in the response to RAI 3.2.2.1.3.2-3-006, not including the interior and exterior support plates in the drip shield shoulder area underestimates the structure rigidity.

In this response, it is demonstrated that including the emplacement pallet in the two-dimensional simulations does not affect the validity of the quasi-static fragility calculations. That is, the stability analyses shown in Table 1 would not change sufficiently to alter the conclusion that the three-dimensional analyses provide a reasonable estimate of drip shield load carrying capacity relative to the two-dimensional dynamic analyses.

The demonstration is carried out in two steps.

1. The loads borne by the stainless steel tubes at the end of a dynamic simulation are quantified and compared to the carrying capacity of the tubes, which are assumed to degrade by general corrosion with time.

2. To estimate the effect of removal of the pallet, the load represented in the two-dimensional dynamic analyses as borne by the pallet is assumed to be applied to the drip shield side legs (i.e., support beams and plates). The resulting moment in the drip shield shoulder is compared with the moment capacity of the drip shield shoulder in order to evaluate if removal of the pallet would result in failure of the stable cases shown in Table 1. Cases where the dynamic analyses predict failure, as noted in Table 1, are not evaluated further.

The analysis of the stainless steel tubes, documented in Section 1.2, shows that the stainless steel tubes will provide support to the drip shield for 30,000 to 50,000 years. It is also shown that in the cases that indicate drip shield stability after strong seismic ground motions, the pallet in the dynamic analysis causes a small overestimate of the drip shield capacity that does not affect the prediction of drip shield stability (Section 1.3). More specifically, removal of the pallet from the dynamic analysis would not result in a prediction of drip shield failure for any cases that are predicted to be stable under comparable quasi-static loads.

1.2 INTERACTION WITH STAINLESS STEEL TUBES

The forces between the drip shield and the emplacement pallet obtained from the numerical simulations are the forces acting on the waste package supports and the stainless steel tubes. The structure and size of the waste package supports are such that they will oppose the drip shield lateral loads without significant deformation.

The interaction between the drip shield and the pallet during strong seismic ground motions is complex. Initially, as shown in Figure 1, the drip shield and the pallet are not in contact. During the early portion of strong ground motions affecting this mechanical system, the drip shield and the pallet will move relative to each other, occasionally physically impacting each other. The impact forces may cause localized damage to the drip shield. Thus, as long as the pallet is free to move inside the drip shield, its presence in the model as an object that can physically impact the drip shield results in an overestimate of damage of the drip shield. The potential beneficial effect of the pallet on the drip shield damage and stability is when the plastic deformation of the drip shield legs is sufficient to allow them to continuously contact the pallet, which then acts as a strut preventing further inward deformation of the drip shield legs. As the strong ground motions continue to cause dynamic lateral loads on the drip shield sides via the rubble, forces between the drip shield and the pallet will typically increase with accumulation of inward plastic deformation. Continued inward deformation of the legs as the strong ground motions continue is a consequence of the fact that: (1) the plastic deformation accumulates with time, and (2) there is no mechanism for reversing the sense of plastic deformation, that is, generally closing the legs due to lateral rubble pressure. As shown in *Mechanical Assessment of Degraded Waste Packages and Drip Shields Subject to Vibratory Ground Motion* (SNL 2007a, Figures 6-60 to

6-62), the main mechanisms of drip shield deformation are either leaning to one side or inward deformation of the legs. Consequently, the forces at the end of the dynamic simulations are adequate for approximating the maximum forces between the pallet and the drip shield that oppose inward deformation of the drip shield legs and its potential collapse. Thus, the forces between the drip shield and the emplacement pallet have been extracted from the end of the dynamic simulations of the drip shield interactions with rubble and used in subsequent analyses discussed below in this RAI response (e.g., Table 2).

The maximum plastic moments in the stainless steel tubes, assuming the formation of three plastic hinges, are listed in Table 2 for all cases noted in Table 1 that did not indicate drip shield failure in the dynamic analyses. As the load on the tubes increases, the plastic hinges will first form on the supports, because the elastic moments at the supports of a rigidly fixed tube are less than at the middle of the tube. As the plastic hinges are formed at the supports, the moments in the middle will increase faster than the moments at the supports, until the plastic hinge is formed in the middle. The moment capacity is calculated as $M = ql^2/16$, where q is the uniformly distributed linear load on the stainless steel tube, and $l = 3.06\,\text{m}$ is the span between the waste package supports as shown in Figure 2. The maximum moments are compared with the plastic moment capacity of the stainless steel (SA-240-S31600) tubes, which are square, with outside dimensions of $6\,\text{in} \times 6\,\text{in}$, and with 0.375-in (9.52-mm) wall thickness (see response to RAI 3.2.2.1.3.2-002, Section 1.2.3). The yield strength of 193 MPa and ultimate tensile strength of 517 MPa for stainless steel at 60°C (SNL 2007a, Section A3) were used to calculate the moment capacities (both plastic and elastic). The moment capacities of the stainless steel tubes will change with time as a result of corrosion. The wall thickness is estimated to decrease due to corrosion at a rate of approximately 1.8 mm (0.07 in) per 10,000 years.

Table 2. Maximum Plastic Moments in the Stainless Steel Tubes due to Interaction with Drip Shield Based on Reaction Forces at the End of Dynamic Simulation

Case	PGV Level (m/s)	Maximum Plastic Moment (kNm)		
		Initial Configuration (15-mm plate thickness)	5-mm-Thinned Configuration (10-mm plate thickness)	10-mm-Thinned Configuration (5-mm plate thickness)
4	2.44	21.3	29.8	2.3
11	2.44	0	39.6	Fails
13	2.44	26.8	26.7	31.1
17	2.44	40.8	7.9	21.9
4	4.07	3.3	9.8	Fails
11	4.07	Fails	Fails	Fails
13	4.07	Fails	Fails	Fails
17	4.07	Fails	49.2	Fails

NOTE: The table entries with “Fails” refer to the failure in the dynamic analysis for that case. These cases were not evaluated further.

The calculated evolution of both the elastic and plastic moment capacities of the stainless steel tubes with time is shown in Figure 4. The linear fit of time to failure, t (years), for a given plastic moment, M (kNm), is:

$$t = 390.494 \times (133.789 - M)$$

The elastic capacities are less representative of the tube response than the plastic capacities, where the applied loads can induce stresses that exceed yield stresses through the entire beam cross section, and are not considered further. The elastic capacities are less representative because the plastic capacity better estimates the maximum load carrying capacity. The plastic capacity relation yields the estimated time periods, listed in Table 3, for which the stainless steel tubes will support the drip shield as represented in the two-dimensional dynamic analysis. Thus, the two-dimensional dynamic analysis adequately represents interaction between the drip shield and the pallet and does not overestimate the drip shield capacity as a result of including the emplacement pallet for at least 33,000 years. Given a nominal drip shield corrosion rate of 51 nm per year (SNL 2007b, Table 8-1[a]), after 50,000 years the drip shield will be thinned by about 2.5 mm. Thus, estimates of mechanical interactions using 5- and 10-mm thinning of the drip shield are improbable.

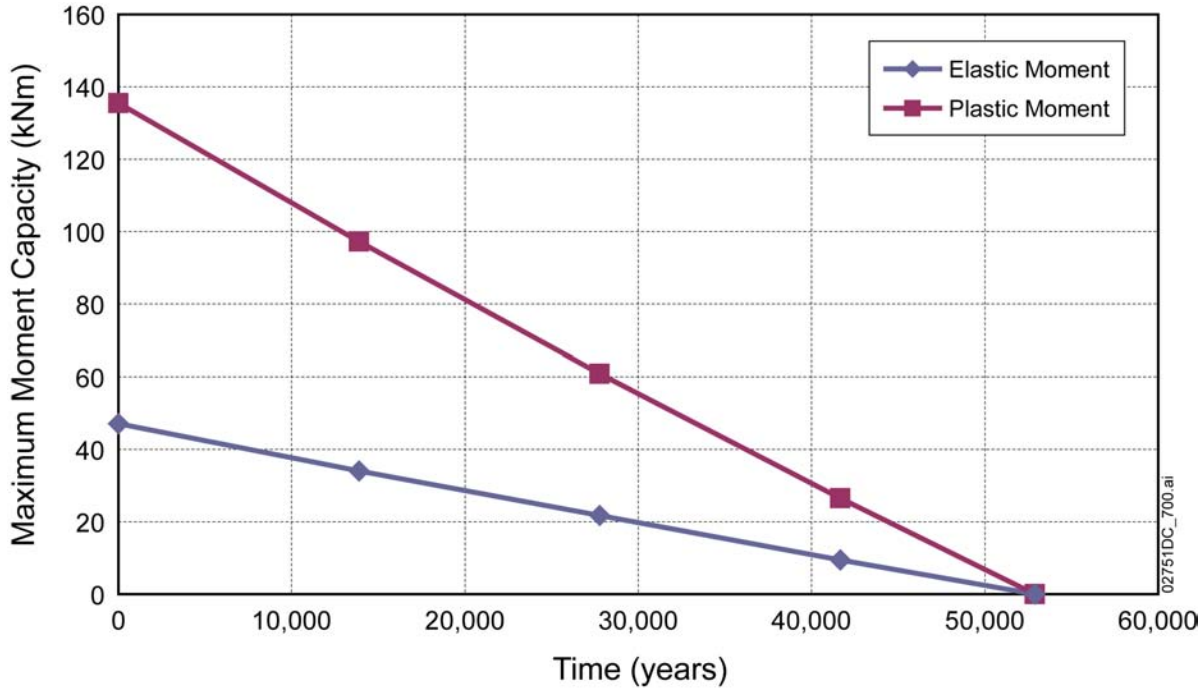

Figure 4. Evolution of the Stainless Steel Tube Moment Capacity with Time

Table 3. Estimated Time Periods for Which the Stainless Steel Tubes Can Sustain the Interaction Forces with a Drip Shield

Case	PGV Level (m/s)	Time Period (Years)		
		Initial Configuration (15-mm plate thickness)	5-mm-Thinned Configuration (10-mm plate thickness)	10-mm-Thinned Configuration (5-mm plate thickness)
4	2.44	43,900	40,600	51,400
11	2.44	No limit	36,800	Fails
13	2.44	41,800	41,800	40,100
17	2.44	36,300	49,200	43,700
4	4.07	51,000	48,400	Fails
11	4.07	Fails	Fails	Fails
13	4.07	Fails	Fails	Fails
17	4.07	Fails	33,000	Fails

NOTE: The table entries with "Fails" refer to the failure in the dynamic analysis for that case. These cases were not evaluated further.

1.3 INTERACTION WITHOUT STAINLESS STEEL TUBES

When the stainless steel tubes completely corrode, after approximately 53,000 years (considering a corrosion rate of 1.8 mm per 10,000 years and a 9.52-mm wall thickness of the stainless steel tubes), only the waste package supports over approximately 20% of the drip shield length can act as struts to prevent potential inward deformation of the drip shield legs. The waste package supports are relatively uniformly distributed along drip shield length, with maximum spacing of approximately 3.06 m, as shown in Figure 2. Thus, the model including the pallets, which is implicitly assumed to extend along the entire length of the drip shield, could overestimate the lateral load bearing capacity for 80% of the drip shield side wall length for time periods longer than 53,000 years.

The forces between the pallet and the drip shield and the rubble loads on the drip shield, as calculated from the two-dimensional analysis, are uniform along the drip shield length. When the stainless steel tubes completely corrode, the drip shield will respond to lateral rubble load as a three-dimensional structure, in which 3.06-m-long spans along the drip shield sides between the waste package supports are unsupported. One consequence of nonuniform support conditions along the drip shield will be that the lateral rubble loads on the drip shield sides will also be nonuniform. The rubble loads and, particularly, the lateral loads are, to a large extent, functions of drip shield wall stiffness and interaction between the drip shield and rubble. A more compliant, unsupported section of the drip shield, which deforms more, will be loaded less than the sections supported by the waste package supports. Thus, the loads on the drip shield sides calculated from the two-dimensional analysis, and used in the following analysis of the effect of removal of the pallet, likely overestimate the rubble loads on the unsupported sections of the drip shield sides.

The lateral rubble loads on the drip shield are transferred by the support beams into: (1) the bulkhead in the crown; (2) the emplacement pallet (if present), which acts as a strut; and (3) the invert, either through the friction between the drip shield legs and rubble (if the drip shield rests on the invert) or directly as the invert rubble accumulates between the drip shield legs below the waste package and the emplacement pallet. In the extreme case, when there is no pallet acting as a strut inside the drip shield and the drip shield is not resting on the invert, the drip shield legs act as cantilevers in response to lateral rubble load. This situation, which is most unfavorable with respect to stability of the drip shield legs and is relatively unlikely, is considered in an estimate of the effect of the lateral rubble load on stability of the drip shield legs along the section of the drip shield without a pallet acting as a strut between the drip shield legs.

1.3.1 Moment Capacity at Top of Drip Shield Support Beam

The moment-curvature curves for the cross section at the top of the support beams (i.e., sidewall shoulder) for three drip shield configurations are shown in Figure 5. The curves are derived assuming bilinear, elasto-plastic material response in the cross section (SNL 2007a, Appendix B). The critical curvature ρ, corresponding to the rupture strain, $\varepsilon_{\max} = 0.164$ (SNL 2007a, Table A-2), is estimated from the formula:

$$\rho = 1/r = \varepsilon_{\max} / y_0$$

where r is the radius of curvature, and y_0 is the distance from the neutral axis. Because the entire height of the cross section at the top of the support beam is between 0.081 and 0.101 m (SNL 2007a, Table B-1), depending on the configuration, and y_0 is less than the height of the cross section, the critical curvature is estimated to be greater than $2\ \mathrm{m}^{-1}$ for the three configurations. Consequently, the critical rupture moments are estimated to be approximately 150, 230, and 320 kNm, for 10-mm-thinned, 5-mm-thinned, and the initial configurations, respectively (Figure 5). These values will underestimate the moment capacity because they do not account for the interior and exterior support plates in the drip shield shoulder area as discussed in the response to RAI 3.2.2.1.3.2-3-006.

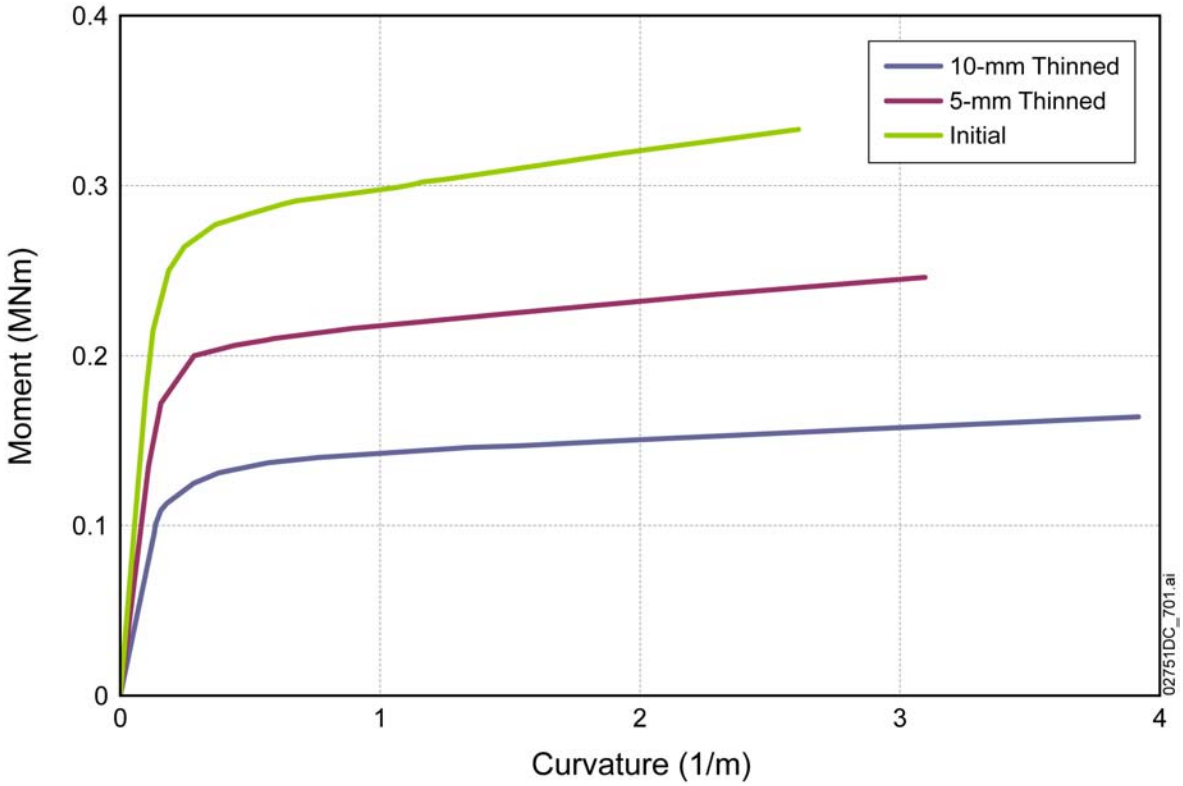

Figure 5. Moment Capacity as a Function of Curvature at the Top of the Support Beam for Three Drip Shield Configurations

1.3.2 Increase of Moment at Top of Drip Shield Support Beam due to Pallet Removal

If a pallet structure does not exist to resist the inward movement of the drip shield side wall under rubble loads, then the load that was resisted by the pallet could be considered to be applied at the side wall and, in the extreme case when the sidewall acts as a cantilever, be resisted by the top of the support beam in the drip shield shoulder area. The upper bounds of additional moments at the top of the support beams as a result of removal of the pallet, assuming that the drip shield legs act as cantilever, are calculated and listed in Table 4. This estimate is based on the interaction forces between the pallet and the drip shield calculated at the end of the dynamic analysis from the two-dimensional model. Again, the moments in Table 4 significantly overestimate the additional moments at the top of the support beams for the following reasons:

- The lateral rubble pressure on the drip shield (and, consequently, the reaction forces between the drip shield and the pallet) calculated from the two-dimensional model overestimates lateral rubble load on the unsupported (by the pallet) section of the drip shield.

- Typically, the drip shield sides do not act as cantilevers. Consequently, a fraction of the interaction force between the pallet and the drip shield will be transferred into the invert as a result of friction between the drip shield and the invert and only a fraction will be transferred to the top of the support beam horizontally supported by the bulkhead.

Table 4. Upper Bounds of Additional Moments at the Top of the Support Beams If the Pallet Is Not Present

Case	PGV Level (m/s)	Moment (kNm)		
		Initial Configuration (15-mm plate thickness)	5-mm-Thinned Configuration (10-mm plate thickness)	10-mm-Thinned Configuration (5-mm plate thickness)
4	2.44	119	167	13
11	2.44	0	222	Fails
13	2.44	150	149	174
17	2.44	229	44	123
4	4.07	18	55	Fails
11	4.07	Fails	Fails	Fails
13	4.07	Fails	Fails	Fails
17	4.07	Fails	276	Fails

NOTE: The table entries with “Fails” refer to the failure in the dynamic analysis for that case consistent with Table 1. These cases were not evaluated further.

1.3.3 Assessment of Drip Shield Stability If Pallet Is Not Present

The moments from Table 4 are added to the existing (residual) moments at the top of the support beams, as calculated at the end of the dynamic simulations, to estimate the resulting moments. Comparing the resulting moments, listed in Table 5, with the critical moments (Section 1.3.1), it is estimated that the removal of the pallet would result in drip shield failure for cases 13 and 17 for 10-mm-thinned configuration at the 2.44 m/s PGV level, and cases 11 and 17 for 5-mm-thinned configuration at the 2.44 m/s and the 4.07 m/s PGV levels, respectively. These cases are in bold in Table 5. However, the quasi-static analyses of the drip shield for these same cases predict failure also, as shown in Table 1. For all other cases, for which the dynamic analysis with the pallet predicts a stable drip shield after strong seismic ground motions, removal of the pallet would not result in a different prediction regarding drip shield stability. Thus, including the pallet in the two-dimensional dynamic analysis of the drip shield overestimates the load bearing capacity of the sections of the drip shield where the pallet is not present, but the overestimation is insufficient to affect the validity of using the quasi-static approach for assessing drip shield fragility.

Table 5. Upper Bounds of Total (residual plus additional) Moments at the Top of the Support Beams If the Pallet Is Not Present

Case	PGV Level (m/s)	Total Moment (pallet contribution + residual) (kNm)		
		Initial Configuration (15-mm plate thickness)	5-mm-Thinned Configuration (10-mm plate thickness)	10-mm-Thinned Configuration (5-mm plate thickness)
Moment Capacity		**320**	**230**	**150**
4	2.44	193 (119 + 74)	214 (167 + 47)	50 (13 + 37)
11	2.44	44 (0 + 44)	**250 (222 + 28)***	Fails
13	2.44	261 (150 + 111)	220 (149 + 71)	**214 (174 + 40)***
17	2.44	270 (229 + 41)	77 (44+ 33)	**174 (123 + 51)***
4	4.07	54 (18+ 36)	78 (55+ 23)	Fails
11	4.07	Fails	Fails	Fails
13	4.07	Fails	Fails	Fails
17	4.07	Fails	**280 (276 + 4)***	Fails

NOTES: "*" denotes that the stability state from dynamic simulations in Table 1 would change from "Stable" to "Fails" under condition of no pallet support.

The table entries with "Fails" refer to the failure in the dynamic analysis for that case consistent with Table 1. These cases were not evaluated further.

1.4 CONCLUSION

The emplacement pallets, including the waste package supports and the stainless steel tubes, which extend along 71% of the drip shield length, will provide support to the drip shield sides during strong seismic ground-motion events for at least 33,000 years as represented in the two-dimensional dynamic analyses. Thus, the two-dimensional analysis does not overestimate drip shield load bearing capacity for 33,000 years. For longer time periods, and particularly after 53,000 years when the stainless steel tubes are expected to be completely corroded, the two-dimensional analysis could overestimate the drip shield load bearing capacity. But this overestimate is compensated to some extent by the interactions with the invert that will resist inward movement of the drip shield legs, which is not included in the structural system evaluation in this RAI response. In addition, this RAI response demonstrates that there is residual strength in the drip shield shoulder area that would resist load that would be applied if the pallet were not present. Taken in aggregate, the overestimate introduced by inclusion of the pallet is not significant and does not affect the validity of the quasi-static approach as a method for assessing drip shield fragility.

2. COMMITMENTS TO NRC

None.

3. DESCRIPTION OF PROPOSED LA CHANGE

None.

4. REFERENCES

SNL (Sandia National Laboratories) 2007a. *Mechanical Assessment of Degraded Waste Packages and Drip Shields Subject to Vibratory Ground Motion.* MDL-WIS-AC-000001 REV 00. Las Vegas, Nevada: Sandia National Laboratories. ACC: DOC.20070917.0006; DOC.20080623.0002; DOC.20081021.0001.

SNL 2007b. *General Corrosion and Localized Corrosion of the Drip Shield.* ANL-EBS-MD-000004 Rev 002 AD 01. Las Vegas, Nevada: Sandia National Laboratories. ACC: DOC.20070807.0004.

SNL 2008. *Features, Events, and Processes for the Total System Performance Assessment: Analyses*. ANL-WIS-MD-000027 REV 00. Las Vegas, Nevada: Sandia National Laboratories. ACC: DOC.20080307.0003; DOC.20080407.0009; LLR.20080522.0166; DOC.20080722.0002.